Theoretical study of Strong gravitational lensing around Dyonic ModMax black hole: constraints from EHT observations

Lola Meliyeva[1,2†] Obid Xoldorov[3‡] Olmos Tursunboyev[4§] Shavkat Karshiboev[5♮] Sardor Murodov[6♯]
Isomiddin Nishonov[7,8¶] Bekzod Rahmatov[9,10♭]

[1]Denou Institute of Entrepreneurship and Pedagogy, Surkhandarya 190500, Uzbekistan
[2]Specialized boarding school, Marvarid Street, Denau 190500, Uzbekistan
[3]Samarkand State University, University Avenue 15, Samarkand 140104, Uzbekistan
[4]Department of Physics, Jizzakh state pedagogical university Jizzakh 130100, Uzbekistan
[5]Uzbek-Finnish Pedagogical Institute, Spitamen Shokh Street 166, Samarkand 140100, Uzbekistan
[6]New Uzbekistan University, Movarounnahr Street 1, Tashkent 100007, Uzbekistan
[7]Physics and Chemistry Department, National Research University TIIAME, Kori Niyoziy 39, 100000 Tashkent, Uzbekistan
[8]Shahrisabz State Pedagogical Institute, Shahrisabz Str. 10, Shahrisabz 181301, Uzbekistan
[9]Tashkent International University of Education, Imom Bukhoriy 6, Tashkent 100207, Uzbekistan
[10]Tashkent State Technical University, Tashkent 100095, Uzbekistan

Abstract: In this study, we investigate the properties of the Dyonic ModMax black hole solution using strong gravitational lensing. Additionally, we calculate the time delay between two relativistic images of a background object. First, we analyze expressions for the photon orbits in the spacetime of the Dyonic ModMax black hole. To obtain observational consequences, we provide expressions for the observable quantities, such as angular radius and magnifications. The numerous observations suggest that many nearby galaxies contain supermassive central black holes. In our model, such a supermassive black hole can be characterized by two additional parameters: γ and Q. Notably, the bending angle $\alpha_D(b)$ and the angular position θ_∞ decrease with increasing charge of the black hole Q, while the parameter γ displays opposite behavior to that of Q. By using observational data of supermassive black holes SgrA* and M87*, we obtain constraints for these parameters.

Keywords: strong gravitational lensing, dyonic modmax black hole, milky way, EHT

DOI: 10.1088/1674-1137/adf4a0 **CSTR:** 32044.14.ChinesePhysicsC.49125102

I. INTRODUCTION

The study of strong gravitational lensing provides a profound window into the nature of spacetime and the properties of black holes. This phenomenon, predicted by Einstein's theory of general relativity [1, 2], occurs when light from a distant source is bent by the gravitational field of a massive object, such as a black hole, thus resulting in multiple images or highly magnified and distorted images of the source [3]. Strong gravitational lensing not only offers insights into the structure and dynamics of black holes but also serves as a powerful tool for probing fundamental physics under extreme conditions [4].

In recent years, the Event Horizon Telescope (EHT) has revolutionized our understanding of black holes by capturing the images of the shadows of supermassive black holes at the center of the galaxy M87* [5, 6] and at the center of the Milky Way [7, 8]. These unprecedented observations provide a unique opportunity to test various black hole models and theories of gravity [9]. Previous research has investigated the lensing properties of black holes in various modified gravity frameworks [10−14]. However, the gravitational lensing effects of black holes described by non-linear electrodynamics, such as the Dyonic ModMax model, remain underexplored.

Recent studies have explored gravitational lensing in non-linear electrodynamics, including the Dyonic ModMax model, placing focus on weak lensing, plasma effects, and black hole shadows [15−20]. However, strong lensing and the interplay of dual charges with rotation re-

Received 21 July 2025; Accepted 22 July 2025; Published online 23 July 2025
† E-mail: lolamelieva9634@gmail.com, ixm207@piima.uz
‡ E-mail: obidxoldorov@gmail.com
§ E-mail: tursunboyevolmosbek5597@gmail.com
♮ E-mail: shavkat.qarshiboyev.89@bk.ru
♯ E-mail: mursardor@ifar.uz
¶ E-mail: isomiddinniwonov96@gmail.com
♭ E-mail: rahmatovbekzod@samdu.uz

main underexplored [21, 22]. The Dyonic ModMax model's duality and conformal invariance offer unique lensing signatures [23, 24]. This study investigates strong lensing in Dyonic ModMax black holes and proposes novel observational tests to constrain model parameters using future telescope data [16, 17], thereby addressing primary and relativistic images in the strong gravitational field regime.

The Dyonic ModMax black hole model extends the conventional Maxwell theory by incorporating a modification through nonlinear electrodynamics, which leads to distinct spacetime features that are absent in other modified gravity models [25]. Among the intriguing models that have emerged is the Dyonic ModMax black hole, which incorporates modifications to Maxwell's electrodynamics that lead to novel predictions about the behavior of light and matter in the vicinity of the black hole [26−28].

This article presents a theoretical investigation of strong gravitational lensing around Dyonic ModMax black holes. We aim to place constraints on the parameters of the Dyonic ModMax black hole model by analyzing and comparing the lensing effects with EHT observations. We begin by reviewing the key aspects of gravitational lensing theory [29] and the Dyonic ModMax black hole solution [30−32]. Subsequently, we derive the lensing observables, such as the angular position and magnification of the lensed images, and examine how these are influenced by the unique features of the Dyonic ModMax black hole.

Our study is motivated by the need to explore alternative gravity theories and to understand how deviations from classical general relativity manifest in observational phenomena [33−41]. The Dyonic ModMax black hole serves as a test case for these explorations by providing insights that could extend to other modified gravity theories. By comparing our theoretical predictions with the empirical data from the EHT [42−51], we aim to identify distinctive signatures of the Dyonic ModMax black hole and determine the feasibility of this model in explaining the observed characteristics of black hole shadows and lensing patterns.

The results of this investigation will not only shed light on the viability of the Dyonic ModMax black hole model but also contribute to the broader effort to test the limits of general relativity and explore new physics in the strong gravity regime [38, 52−55]. Through this theoretical and observational synergy, we seek to deepen our understanding of black holes and the fundamental laws governing our universe [56−58].

In this paper, we estimate the deflection angle of the light rays and the time delay of the signals from two relativitic images. We show that time delays between relativistic images are indeed measurable in most supermassive black holes cases. Moreover, we learn that in a first approximation, the time delay between consecutive relativistic images is proportional to the minimum impact angle. The ratio between these two observables is merely the distance of the lens, which can be estimated following precise guidelines and without bias. This paper is structured as follows: in Sect. II, we briefly explain the Dyonic ModMax black hole solution and obtain horizon properties. In Sect. III, we provide the main results of the gravitational lensing in the case of strong field regime. In Sect. IV, we derive a general expression for the time delay as well as consider the Dyonic ModMax spacetime case and calculate the time delay for supermassive black holes at the center of several galaxies such as Milky Way, M87, NGC4649, NGC4697, and NGC5128(cenA). Finally, Sect. V concludes the paper.

II. HORIZON PROPERTIES OF DYONIC MODMAX BLACK HOLE

Dyonic ModMax black hole space-time singularities have been extensively studied in GR with NED [17, 28, 59−61]. However, here we focus on a new black hole solution in GR with NED using an exotic field referred to as the Dyonic ModMax field. The action can be written as

$$S = \int \sqrt{-g}\left[\frac{1}{8\pi\kappa}R + L(x,y)\right]\mathrm{d}^4x, \tag{1}$$

where

$$L(x,y) = x\cosh\gamma + \sqrt{x^2+y^2}\sinh\gamma, \qquad \text{where} \tag{2}$$

$$x = \frac{1}{4}F_{\mu\nu}F^{\mu\nu} \qquad \text{and} \qquad \mathrm{y} = \frac{1}{4}\mathrm{F}_{\mu\nu}\tilde{\mathrm{F}}^{\mu\nu} \tag{3}$$

are the electromagnetic Lorentz invariants in terms of the electromagnetic tensor $F_{\mu\nu}$ and its dual $\tilde{F}_{\mu\nu} := \frac{1}{2}\epsilon_{\mu\nu\sigma\rho}F^{\sigma\rho}$. From the ModMax Lagrangian, the Plebański dual variable reads [30, 62]

$$P_{\mu\nu} := -L_xF_{\mu\nu} - L_y\tilde{F}_{\mu\nu} = \left[\cosh\gamma - \frac{x}{(x^2+y^2)^{1/2}}\sinh\gamma\right]F_{\mu\nu} - \frac{y\sinh\gamma}{(x^2+y^2)^{1/2}}\tilde{F}_{\mu\nu}.$$

Its dual is

$$\tilde{P}_{\mu\nu} = \left[\cosh\gamma - \frac{x}{(x^2+y^2)^{1/2}}\sinh\gamma\right]\tilde{F}_{\mu\nu} + \frac{y\sinh\gamma}{(x^2+y^2)^{1/2}}F_{\mu\nu}.$$

The modified Maxwell field equation is given by

$$\nabla_\mu P^{\mu\nu} = 0. \tag{4}$$

Additionally, the Einstein equations can be expressed as

$$R^\mu_\nu - \frac{1}{2}\delta^\mu_\nu R + \Lambda\delta^\mu_\nu = 8\pi T^\mu_\nu. \tag{5}$$

Here, the energy momentum tensor T^μ_ν is given by [30]

$$8\pi T^\mu_\nu = -F^{\mu\beta}P_{\beta\nu} + \delta^\mu_\nu L = F^{\mu\beta}(L_x F_{\beta\nu} + L_y \tilde{F}_{\beta\nu}) + \delta^\mu_\nu L. \tag{6}$$

To solve the Einstein equation, we choose following anzats:

$$\mathrm{d}s^2 = -f(r)\mathrm{d}t^2 + f(r)^{-1}\mathrm{d}r^2 + r^2(\mathrm{d}\theta^2 + \sin^2\theta\mathrm{d}\phi^2). \tag{7}$$

In this paper, we consider only asymptotically flat configurations; therefore, we choose $\Lambda = 0$ in Eq. (5). First we take $A_\mu = (\Phi(r), 0, 0, Q_m\cos\theta)$ to consider the dyonic solution. In this case, we get

$$F_{\mu\nu} = -\Phi_{I,r}\delta^0_{[\mu}\delta^1_{\nu]} - Q_m\sin\theta\delta^2_{[\mu}\delta^3_{\nu]}. \tag{8}$$

Therefore,

$$x = \frac{1}{2}\left(-\Phi^2_{,r} + \frac{Q_m^2}{r^4}\right),\ y = -\frac{\Phi_{,r}Q_m}{r^2},$$
$$(x^2+y^2)^{1/2} = \frac{1}{2}\left(-\Phi^2_{,r} + \frac{Q_m^2}{r^4}\right), \tag{9}$$

and it is straightforward to show that the only non-vanishing Pleban'ski variables are

$$P_{01} = -(\cosh\gamma + \sinh\gamma)\Phi_{,r} = -\mathrm{e}^{\gamma}\Phi, r,$$
$$P_{23} = -(\cosh\gamma - \sinh\gamma)Q_m\sin\theta = -\mathrm{e}^{-\gamma}Q_m\sin\theta. \tag{10}$$

We can express the electric potential as

$$\Phi(r) = \frac{Q_e\cdot\mathrm{e}^{-\gamma}}{r}. \tag{11}$$

This condition sets a conservation low for P_{01}. In this case, the gravitational field equations read

$$-\frac{m_{,r}}{r^2} = -\frac{(Q_e^2+Q_m^2)\cdot\mathrm{e}^{-\gamma}}{2r^4},$$
$$-\frac{m_{,rr}}{2r} = \frac{(Q_e^2+Q_m^2)\cdot\mathrm{e}^{-\gamma}}{2r^4}, \tag{12}$$

and the solution of this system of equations is

$$m(r) = M - \frac{(Q_e^2+Q_m^2)\cdot\mathrm{e}^{-\gamma}}{2r}. \tag{13}$$

Finally, we can find the lapse function of the metric Eq.(7):

$$f(r) = 1 - \frac{2M}{r} + \frac{(Q_\mathrm{e}^2+Q_m^2)\cdot\mathrm{e}^{-\gamma}}{r^2}, \tag{14}$$

where Q_e and Q_m are the electric and magnetic charge of the black hole, respectively, and γ is related to a constant screening factor for the charge of the black hole, which corresponds to the nonlinear parameter [32]. If we choose $\gamma = 0$, Maxwell's theory is recovered. Additionally, by choosing $Q_e = Q_m = 0$ the Schwarzschild case is easily obtained. To analyze the horizon properties of such a black hole, we set $f(r) = 0$. Under this condition, the event horizon can be determined using the following expression:

$$r_h = M \pm \sqrt{\left(M^2 - (Q_e^2+Q_m^2)\cdot\mathrm{e}^{-\gamma}\right.}. \tag{15}$$

This paper examines only the motion of a photon, which is a neutral, massless particle. Thus, we can define Q as $Q_\mathrm{e}^2 + Q_m^2 = Q^2$. We can obtain the maximum value of black hole charge using Eq. (15) as follows:

$$0 < Q < M\cdot\mathrm{e}^{-\gamma/2}. \tag{16}$$

Eq. (15) thus clearly indicates that the Q and γ parameters negatively affect the horizon radius, and Eq. (16) provides the boundary values for charge Q in terms of M and γ.

III. STRONG GRAVITATIONAL LENSING OF DYONIC MODMAX BLACK HOLE

This section investigates the strong gravitational lensing effect in the spacetime described in Eq. (7). The photon sphere radius can be determined using the following expression [63]:

$$\frac{g'_{\theta\theta}(r)}{g_{\theta\theta}(r)} - \frac{g'_{tt}(r)}{g_{tt}(r)} = 0, \tag{17}$$

where $'$ is the differentiation with respect to the radial coordinate r. From Eqs. (7) and (17), we get

$$r_m = \frac{3M + \sqrt{9M^2 - 8Q^2\mathrm{e}^{-\gamma}}}{2}. \tag{18}$$

The specific energy and angular momentum can be written as

$$E \equiv -g_{\mu\nu}t^{\mu}\kappa^{\nu} = \frac{\Delta}{r^2}\dot{t}, \tag{19}$$

and

$$L \equiv g_{\mu\nu}\phi^{\mu}\kappa^{\nu} = r^2\dot{\phi}, \tag{20}$$

where $\Delta = f(r)\cdot r^2$ and κ_{μ} is the killing vector. The impact parameter is an important quantity and is defined as

$$b \equiv \frac{L}{E} = \frac{r^4\dot{\phi}}{\Delta\dot{t}}. \tag{21}$$

Additionally, we assume that the motion occurs in the equatorial plane, $\theta = \pi/2$. Under this assumption, the equations of motion in the radial direction can be obtained as

$$\dot{r}^2 = \frac{\Delta^2}{r^4}\dot{t}^2 - \Delta\dot{\phi}^2, \tag{22}$$

or

$$\dot{r}^2 = V(r), \tag{23}$$

where $V(r)$is the effective potential for the motion of the photon and is expressed as

$$V(r) \equiv \mathrm{e}^2 - \frac{\Delta}{r^4}L^2. \tag{24}$$

We consider that the light beam coming from infinity is deflected at the closest distance $r = r_0$ and travels to infinity. At the closest distance, $\dot{r}$ vanishes and the following formula is obtained from Eq. (22) for the critical impact parameter at the closest distance: [63]

$$b(r_0) = \frac{r_0^2}{\sqrt{\Delta(r_0)}}. \tag{25}$$

Using the above equation, we can define the critical impact parameter as

$$b_c(r_m) \equiv \lim_{r_0\to r_m} b(r_0) = \lim_{r_0\to r_m}\frac{r_o^2}{\sqrt{\Delta(r_0)}}. \tag{26}$$

The critical impact parameter is defined such that photons with an impact parameter of $b < b_c$ fall into the black hole. Parameter $b(r_0)$ can be expanded in the power of $r_0 - r_m$ as

$$b(r_0) = b_c(r_m) + \frac{3Mr_m - 4Q^2\mathrm{e}^{-\gamma}}{2(Mr_m - \epsilon M^2)^{\frac{3}{2}}}(r_0 - r_m)^2 + O((r_0 - r_m)^3). \tag{27}$$

From Eq. (22), we can establish the following relationship between r and ϕ:

$$\left(\frac{\mathrm{d}r}{\mathrm{d}\phi}\right)^2 = r^4\left(\frac{1}{b^2} - \frac{\Delta}{r^4}\right), \tag{28}$$

which can alternatively be expressed in terms of the deflection angle $\alpha(r_0)$ of the light beam as

$$\alpha = I(r_0) - \pi, \tag{29}$$

where

$$I(r_0) \equiv 2\int_{r_0}^{\infty}\frac{\mathrm{d}r}{r^2\sqrt{\frac{1}{b^2} - \frac{\Delta}{r^4}}}. \tag{30}$$

By introducing a variable z, defined as

$$z \equiv 1 - \frac{r}{r_0}, \tag{31}$$

$I(r_0)$ can be rewritten as

$$I(r_0) = \int f(z, r_0)\mathrm{d}z, \tag{32}$$

where

$$f(z, r_0) = \frac{2r_0}{\sqrt{c_1(r)z + c_2(r_0)z^2 + c_3(r_0)z^3 + c_4(r_0)z^4}}, \tag{33}$$

$$c_1(r_0) \equiv 2(r_0^2 - 3Mr_0 + 2Q^2\mathrm{e}^{-\gamma}), \tag{34}$$

$$c_2(r_0) \equiv -r_0^2 + 6Mr_0 - 6Q^2\mathrm{e}^{-\gamma}, \tag{35}$$

$$c_3(r_0) \equiv -2Mr_0 + 46Q^2\mathrm{e}^{-\gamma}, \tag{36}$$

$$c_4(r_0) \equiv -Q^2\mathrm{e}^{-\gamma}. \tag{37}$$

$I(r_0)$ can be split into two parts, *i.e.*, a divergent part $I_D(r_0)$ and a regular part $I_R(r_0)$: $I(r_0) = I_D(r_0) + I_R(r_0)$. The divergent part is expressed as

$$I_D(r_0) = \int_0^1 f_D(z, r_0)\,\mathrm{d}z, \tag{38}$$

where

$$f_D(z,r_0)=\frac{2r_0}{\sqrt{c_1(r_0)z+c_2(r_0)z^2}}, \tag{39}$$

and the result is

$$I_D(r_0)=\frac{4r_0}{\sqrt{-r_0^2+6Mr_0-6Q^2\mathrm{e}^{-\gamma}}} \log\frac{\sqrt{-r_0^2+6Mr_0-6Q^2\mathrm{e}^{-\gamma}}+\sqrt{r_0^2-2Q^2\mathrm{e}^{-\gamma}}}{2(r_0^2-3Mr_0+2Q^2\mathrm{e}^{-\gamma})}. \tag{40}$$

In the strong deflection limit $r_0\to r_m$, Eq. (40) is expressed as

$$I_D(b)=-\bar{a}\log\left(\frac{b}{b_c}-1\right)+\bar{a}\log\frac{2(3Mr_m-4Q^2\mathrm{e}^{-\gamma})}{Mr_m-Q^2\mathrm{e}^{-\gamma}}+ O((b-b_c)\log(b-b_c)), \tag{41}$$

where $\bar{a}$ is given by

$$\bar{a}=\frac{r_m}{\sqrt{3Mr_m-4Q^2\mathrm{e}^{-\gamma}}}. \tag{42}$$

Additionally, the regular part I_R is defined as

$$I_R(r_0)\equiv\int_0^1 f_R(z,r_0)\,\mathrm{d}z, \tag{43}$$

where

$$f_R(z,r_0)\equiv f(z,r_0)-f_D(z,r_0). \tag{44}$$

As we are investigating the deflection angle in the strong field limit $r_0\to r_m$, we consider

$$\lim_{r_0\to r_m} f_R(z,r_0)=\frac{2r_m}{z\sqrt{c_2(r_m)+c_3(r_m)z+c_4(r_m)z^2}}-\frac{2r_m}{z\sqrt{c_2(r_m)}}. \tag{45}$$

Following some calculations, the analytical expression can be written as

$$I_R(b)=\bar{a}\log\left[\frac{4(3Mr_m-4Q^2\mathrm{e}^{-\gamma})^2}{M^2r_m^2(Mr_m-Q^2\mathrm{e}^{-\gamma})}\times(2\sqrt{Mr_m-Q^2\mathrm{e}^{-\gamma}} -\sqrt{3Mr_m-4Q^2\mathrm{e}^{-\gamma}})^2\right]+O((b-b_c)\log(b-b_c)). \tag{46}$$

Eventually, the bending angle of the light rays $\alpha(b)$ in the strong deflection limit $b\to b_c$ is given by [63]

$$\alpha(b)=-\bar{a}\log\left(\frac{b}{b_c}-1\right)+\bar{b}+O\Big((b-b_c)\log(b-b_c)\Big), \tag{47}$$

where $\bar{a}$ and $\bar{b}$ are expressed as

$$\bar{a}=\frac{r_m}{\sqrt{3Mr_m-4Q^2\mathrm{e}^{-\gamma}}} \tag{48}$$

$$\bar{b}=\bar{a}\log\left[\frac{8(3Mr_m-4Q^2\mathrm{e}^{-\gamma})^2}{M^2r_m^2(Mr_m-Q^2\mathrm{e}^{-\gamma})^2}\times \left(2\sqrt{Mr_m-M^2}-\sqrt{3Mr_m-4Q^2\mathrm{e}^{-\gamma}}\right)^2\right]-\pi, \tag{49}$$

respectively. Table 1 lists values for b_c/M, where $\bar{a}$ and $\bar{b}$denote the lensing coefficients as functions of the charge of the black hole Q/M and γ parameters. When the black hole is non-charged ($Q/M=0$), we obtain $b_c=3\sqrt{3}M$, $\bar{a}=1$, and $\bar{b}=-0.40023$. When $Q/M=0.6$, we obtain $b_c=4.59M$, $\bar{a}=1.1092$ and $\bar{b}=-0.4085$, which indicates that in the case of the Dyonic ModMax black hole, the quantity b_c will be smaller than that for the Schwarzschild case. Fig. 1 indicates that coefficient $\bar{a}$increases while $\bar{b}$, b_c, r_m decrease with increasing values of Q/M. Fig. 2 shows the deflection angle $\alpha_D(b)$ as a function of b for different values of Q/M and γ. The deflection angle for Dyonic ModMax black holes (see Fig. 2) monotonically decreases with the impact parameter b and the deflection angle $\alpha_D(b)\to\infty$ as $b\to b_c$. Notably, the deflection angle for Dyonic ModMax black holes decreases with increasing values of b. By contrast, for an impact parameter whose value is similar to the critical impact parameter (see Fig. 2), the deflection angle $\alpha_D(b)$ decreases for increasing values of both Q/M and γ:

$$\beta=\theta-\frac{D_{LS}}{D_{OS}}\Delta\alpha_n. \tag{50}$$

Table 1. Estimated for the strong lensing coefficients $\bar{a}$, $\bar{b}$ and the critical impact parameter b_c/R for Dyonic ModMax Black hole Spacetime. The values for $Q/M=0$ and $\gamma=0$ correspond to a Schwarzschild black hole.

γ	Q/M	$\bar{a}$	$\bar{b}$	b_c/R_s
0	0.0	1	-0.40023	2.59808
-0.5	0.4	1.03512	-0.396203	2.47728
-0.5	0.8	1.58337	-1.08685	1.94022
0.0	0.4	1.01974	-0.397184	2.49912
0.0	0.8	1.12317	-0.413638	2.27299
0.5	0.4	1.01147	-0.398215	2.55523
0.5	0.8	1.05727	-0.396916	2.41483

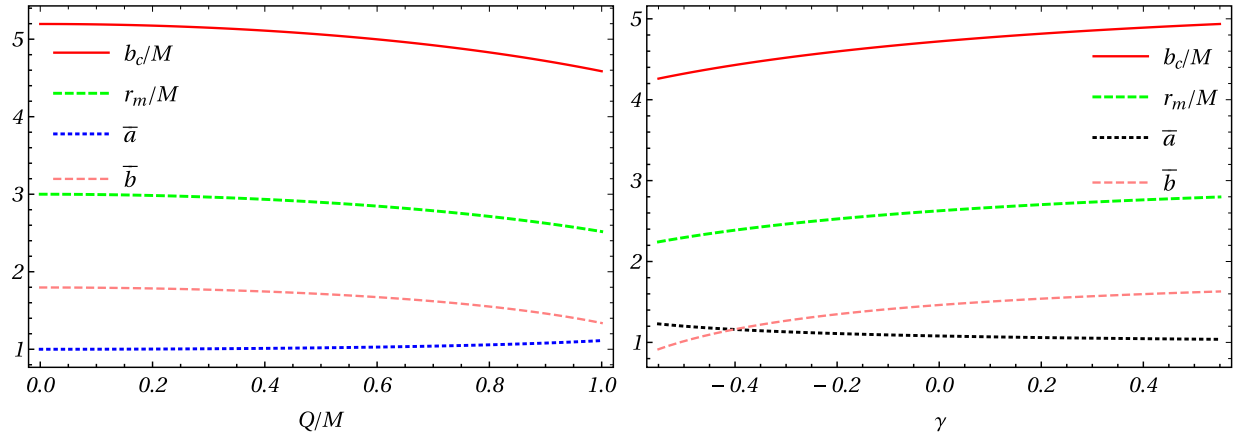

Fig. 1. (color online) Quantities $b_c/M, r_m/M, \bar{a}$, and $\bar{b}$ in the Dyonic ModMax spacetime as functions of Q/M and γ. $\bar{a}=1$ and $\bar{b}=-0.4002$ at $Q/M=0, \gamma=0$ correspond to the values of a Schwarzschild black hole.

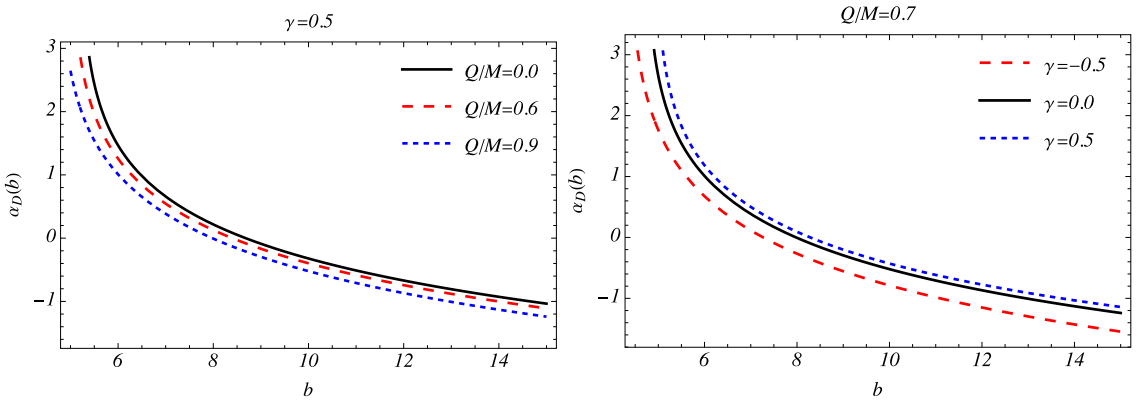

Fig. 2. (color online) Variation in deflection angle for Dyonic ModMax black hole spacetime as a function of the impact parameter b for different values of Q/M(left) and γ (right).

Here, $\Delta\alpha=\alpha-2n\pi$ is the offset of the deflection angle looping over $2n\pi$ and n is an integer; β is the angular position of the source and θ is the angular position of the image from the optic axis. The distance between the observer and the lens and between the observer and the source are denoted by D_{OL} and D_{OS}, respectively. Using Eqs. (47) and (50), the position of the nth relativistic image can be approximated as [63]

$$\theta_n=\theta_n^0+\frac{b_c e_n(\beta-\theta_n^0)D_{OS}}{\bar{a}D_{LS}D_{OL}}, \tag{51}$$

where

$$e_n=\mathrm{e}^{\left(\frac{\bar{b}}{\bar{a}}-\frac{2n\pi}{\bar{a}}\right)}. \tag{52}$$

θ_n^0 denotes the image positions corresponding to $\alpha=2n\pi$. As gravitational lensing conserves surface brightness, the magnification is the quotient of the solid angles subtended by the nth image and the source ([63−65]). The magnification of the nth relativistic image is expressed as [63]

$$\mu_n=\left(\frac{\beta}{\theta}\frac{d\beta}{d\theta}\right)^{-1}=\frac{b_c^2 e_n(1+e_n)D_{OS}}{\bar{a}\beta D_{LS}D_{OL}^2}. \tag{53}$$

The first relativistic image is the brightest one, and the magnifications decrease exponentially with n. The magnifications are proportional to $1/D_{OL}^2$, which is a very small factor and thus causes the relativistic images to be very faint, unless the value of β is close to zero, *i.e.*, nearly perfect alignment. Having obtained the deflection angle (Eq. (47), (48), and (49)), we calculate three observables of relativistic images (see Table 3, Fig. 3, 4 and 5), the angular position of the asymptotic relativistic images (θ_∞), the angular separation between the outermost and asymptotic relativistic images(s_∞), (see Fig. 4) and the relative magnification of the outermost relativistic image with respect to the other relativistic images (r_{mag})(see Fig. 5) [63].

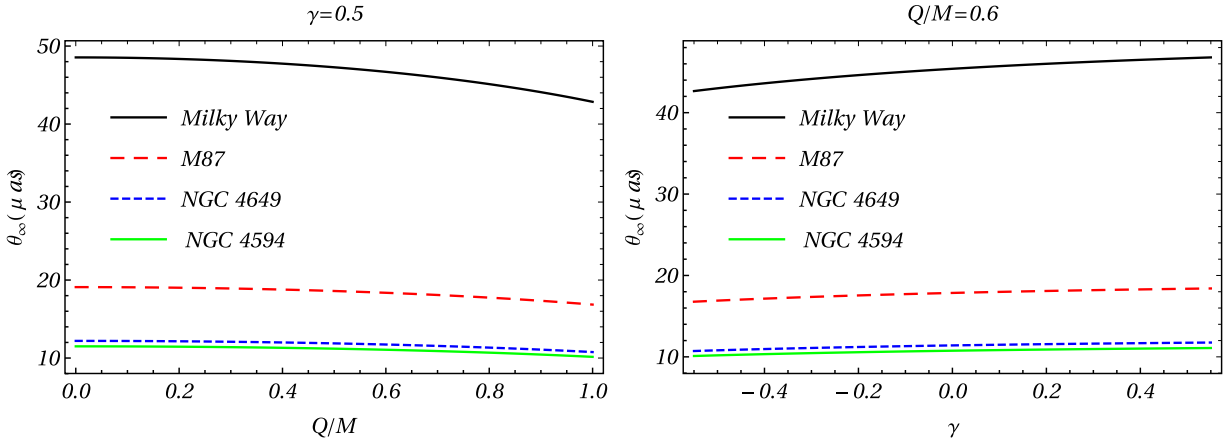

Fig. 3. (color online) Behavior of lensing observables θ_∞ as a function of parameters Q/M and γ in the strong field limit obtained by considering the spacetime around the compact object.

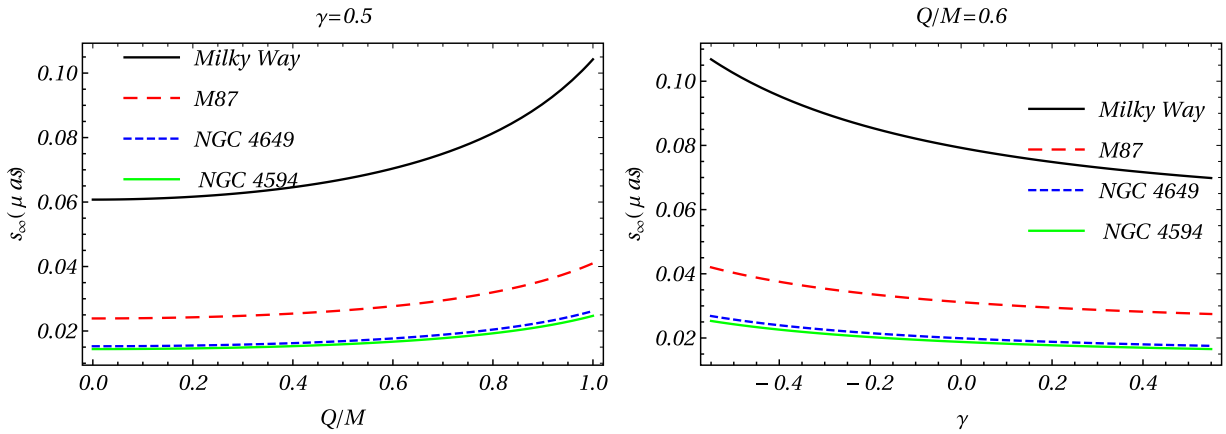

Fig. 4. (color online) Behavior of lensing observables s_∞ as a function of parameters Q/M and γ in the strong field limit obtained by considering the spacetime around the compact object.

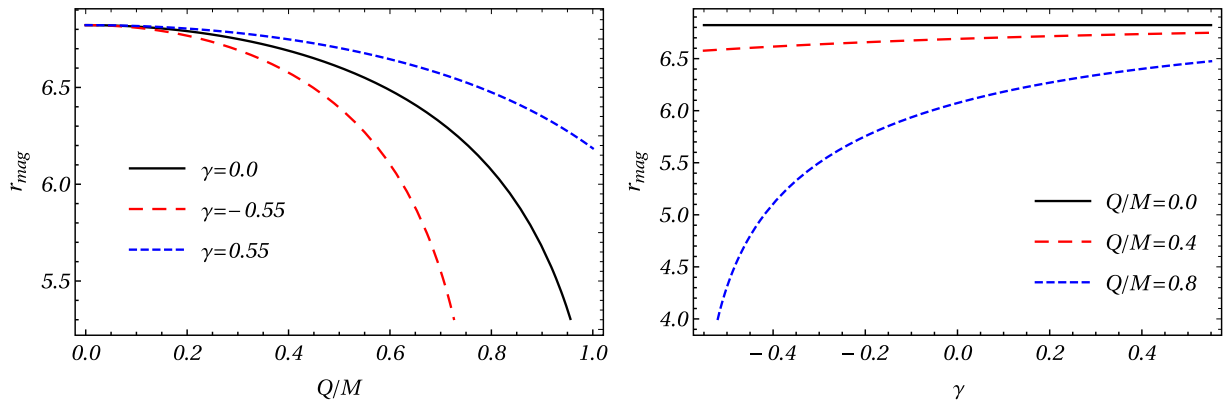

Fig. 5. (color online) Graph illustrating the relationship between the contact parameter $r_{\rm mag}$ and the parameter ϵ.

$$\theta_\infty = \frac{b_c}{D_{OL}}, \tag{54}$$

$$s = \theta_1 - \theta_\infty = \theta_\infty \mathrm{e}^{\left(\frac{\bar{b}}{\bar{a}} - \frac{2n\pi}{\bar{a}}\right)}, \tag{55}$$

$$r_{\rm mag} = \frac{5\pi}{\bar{a}\log 10}. \tag{56}$$

The strong deflection limit coefficients $\bar{a}$, $\bar{b}$ and the critical impact parameter values can be obtained using the measured values of s, $r_{\rm mag}$, and θ_∞. If θ_∞ represents the

Table 2. Angular position of asymptotic relativistic images (θ_∞), angular separation between the outermost and asymptotic relativistic images (s_∞), and relative magnification of the outermost relativistic image with respect to other relativistic images ($r_{\rm mag}$) for Milky Way, NGC4486, and NGC4649 for the case in which the charge of the black hole Q/M and γ parameters are fixed.

γ	Q/M	Milky Way		NGC4486		NGC4649		$r_{\rm mag}$
		$\theta_\infty(\mu as)$	$S(\mu as)$	$\theta_\infty(\mu as)$	$S(\mu as)$	$\theta_\infty(\mu as)$	$S(\mu as)$	
0.0	0.0	48.5447	0.0607535	19.0935	0.0238954	12.1986	0.0152665	6.82188
-0.5	0.4	46.2876	0.0729555	18.2057	0.0286946	11.9974	0.0183327	6.59044
-0.5	0.8	36.2528	0.345028	14.2589	0.135705	11.3382	0.0867007	4.30845
0.0	0.4	47.2071	0.067439	18.5674	0.0265249	11.8625	0.0169465	6.68985
0.0	0.8	42.4706	0.109304	16.7044	0.0429911	10.6723	0.0274666	6.07378
0.5	0.4	47.744	0.0645842	18.7786	0.0254021	11.9974	0.0162291	6.74453
0.5	0.8	45.1208	0.081358	17.7468	0.0319995	11.3382	0.0204441	6.45234

Table 3. Time delay between two relativistic images of different galaxies.

Galaxy	$M(M_\odot)$	D_{OL}(Mpc)	M/D_{OL}	$\Delta T^S_{2,1}(Schw)$	$\Delta T^S_{2,1}(DM)$
Milky Way	3.61×10^6	0.00762	2.26467×10^{-11}	11.4968	8.748
"NGC4486(M87)"	3.0×10^9	16.1	8.90733×10^{-12}	8021	7270
NGC4649	2.0×10^9	16.8	5.6908×10^{-12}	8021	7270
NGC4697	1.7×10^8	11.7	6.94569×10^{-13}	5347.34	4846.67
NGC5128(cenA)	2.4×10^8	4.2	2.73158×10^{-12}	454.53	411.97

asymptotic position of a set of images in the limit $n\to\infty$, then we consider that only the outermost image θ_1 is resolved as a single image and all the remaining images are packed together at θ_∞. The measured values can be compared with those predicted by the theoretical models to check the nature of the black hole. Table 3 lists the observable values corresponding to various values of γ and Q. The results indicate that the Dyonic ModMax black hole exhibits unique and distinguishable observable characteristics compared to other configurations.

One of the important conclusions in the study of deflection angle is that we can constrain the Dyonic ModMax spacetime parameter using EHT observation. Eq. (54) can be used to ascertain the specific values of these parameters that may be used to align the diameters of the M87* and Sgr A* BH, as determined by EHT. The angular size of the image of BH M87* is reported to be $\theta_d = 42\pm3$ μas. The mass and distance of M87* from the solar system is $M = 6.5\times10^9 M_\odot$ and $d = 16.8$ Mpc, respectively [7, 66]. The constraints on M87* are depicted in the left panel of Fig. 6, which reveals a limited boundary region for the charge for negative values of γ , and a significantly larger region for positive values of γ. More specificly, the parameter constraints are $0.7\geq Q>0.4$ and $\gamma\geq-0.5$. The observational data of the supermassive BH Sgr A* may be analyzed using the same methodology. A study conducted by Akiyama *et al.* (2019) determined that the angular diameter of the shadow of the BH Sgr A* is approximately $\theta_d = 48.7\pm7\mu$as with an approximate mass of $M\simeq4\times10^6 M_\odot$. The distance from Earth is approximately $d\simeq8$kpc. The results for Sgr A* are shown in the right panel of Fig. 6. The graph indicates that the allowed parameter region for Sgr A* is broader compared to that of M87*, namely $Q\geqslant0.3$ and $\gamma\geqslant-0.5$. This broader range can likely be attributed to the greater observational uncertainties associated with Sgr A*.

IV. TIME DELAY IN STRONG FIELD LIMIT

The time difference is caused by the photons taking different paths as they wind the black hole, thus leading to a time delay between different images. If the time signals of the first image and other packed images can be distinguished, then the time spent by the photon to wind around the black hole is given by [67]

$$\tilde{T}(b) = \bar{a}\log\left(\frac{b}{b_c}-1\right)+\bar{b}+O(b-b_c). \tag{57}$$

As the images are highly demagnified, and the separation between the images is of the order of microarcseconds, we must at least distinguish the outermost relativistic image from the rest. Additionally, we assume the source to be variable, which generally is abundant in all galaxies; otherwise, there is no time delay to measure. For spherically symmetric black holes, the time delay between the first and second relativistic image is expressed as [67]

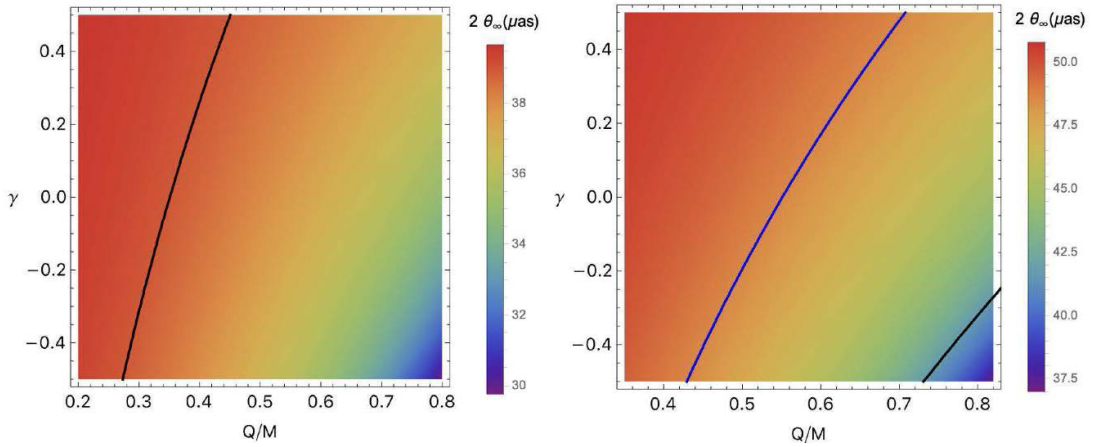

Fig. 6. (color online) Constraining parameter obtained using EHT observation for M87* (left panel) and SgrA*(right panel). The black thick line corresponds to the maximum parameter values and is consistent with the observational results of 39 μas for M87*(left panel) and 41.7 μas for SgrA*(right panel), while the blue line represents the middle value of the observational results (48.7 μas for SgrA*).

$$\Delta T^{s}_{2,1} = 2\pi b_c = 2\pi D_{OL}\theta_{\infty}. \tag{58}$$

Using Eq. (58), if we can measure the time delay accurately and the critical impact parameter with negligible error, we can obtain the distance of the black hole accurately.Table 3 compares several galaxies representing Schwarzschild and Dyonic ModMax spacetime. In the Dyonic ModMax spacetime, the time delays $\Delta T^{s}_{2,1}$ between two distinct relativistic images are comparatively smaller than the fixed value of Q/M and γ in the Schwarzschild cases. We have also analytically derived the time delays $\Delta T^{s}_{2,1}$ between the first and second-order relativistic images for various astronomical objects including the Milky Way, M87, NGC4649, NGC4697, and NGC5128(cenA) with the help of data obtained from Ref. [65]. Using this analysis, we have shown that if we have an independent observation for the time delay, we can strongly constrain the Dyonic ModMax space time parameters Q and γ owing to a distinguishable difference in the measured time delay.

V. CONCLUSION

We draw the following conclusions through this investigation:

- The radius of the spherical photon orbit r_m, the critical impact parameter b_c, the lensing coefficient $\bar{b}$, the deflection angle $\alpha_D(b)$, and the angular position θ_{∞} decrease with increasing values of Q, while the lensing coefficient $\bar{a}$ and angular separation s_{∞} exhibit the opposite trend. Consequently, the parameter γ behaves inversely to Q.
- Additionally, we illustrated the constraining in the Dyonic ModMax spacetime with EHT observations using parametric space graphs.
- We analytically derived the time delays $\Delta T^{s}_{2,1}$ between first and second-order relativistic images for the Milky Way, M87, NGC4649, NGC4697, and NGC5128(cenA). We conclude that the time delay is larger for supermassive black holes of higher mass as compared to lighter black holes.
- Graphical and tabular results revealed the dependence of the deflection angle on parameters Q and γ. Notably, when γ is negative, the deflection angle decreases more sharply, while positive values of γ tend to smooth out this variation. EHT observations, especially those related to the shadow diameters of the M87* and SgrA* black holes, were used to establish experimental constraints on these parameters. For M87*, the parameters are constrained by $0.7 \geq Q > 0.4$ and $\gamma \geq -0.5$, whereas for SgrA*, the allowed parameter space is broader, i.e $Q \geqslant 0.3$ and $\gamma \geqslant -0.5$, due to larger observational uncertainties.

References

[1] C. M. Will, Living Rev. Relativ. **9**, 3 (2006)
[2] C. M. Will, Living Rev. Relativ. **17**, 4 (2014)
[3] P. Schneider, J. Ehlers, and E. E. Falco, Gravitational Lenses. 1992.
[4] M. Bartelmann, Class. Quantum Grav. **27**, 233001 (2010)
[5] K. Akiyama and *et al.* (Event Horizon Telescope Collaboration), Astrophys. J. **910**, L12 (2021)
[6] K. Akiyama and *et al.* (Event Horizon Telescope Collaboration), Astrophys. J. **910**, L13 (2021)
[7] K. Akiyama and *et al.* (Event Horizon Telescope Collaboration), Astrophys. J. **875**, L1 (2019)
[8] K. Akiyama and *et al.* (Event Horizon Telescope Collaboration), Astrophys. J. **875**, L3 (2019)
[9] C. Goddi, H. Falcke, M. Kramer *et al.*, Int. J. Mod. Phys. D **26**, 1730001 (2017)
[10] X. Jiang, X. Ren, Z. Li *et al.*, Mon. Not. R. Astron. Soc.

528, 1965 (2024)
[11] X.-M. Kuang, Z.-Y. Tang, B. Wang *et al.*, Phys. Rev. D **106**, 064012 (2022)
[12] S.-S. Zhao and Y. Xie, European Physical Journal C **77**, 272 (2017)
[13] S. Chen and J. Jing, Class. Quantum Grav. **27**, 225006 (2010)
[14] T. L. Smith, arXiv: 0907.4829
[15] A. Ditta, X. Tiecheng, F. Atamurotov *et al.*, Chin. J. Phys. **83**, 664 (2023)
[16] R. C. Pantig, L. Mastrototaro, G. Lambiase *et al.*, Eur. Phys. J. C **82**(12), 1155 (2022)
[17] S. I. Kruglov, Int. J. Mod. Phys. D **31**(04), 2250025 (2022)
[18] Z. Turakhonov, F. Atamurotov, A. Ovgun *et al.*, Commun. Theor. Phys. **76**(11), 115401 (2024)
[19] B. Rahmatov, M. Zahid, S. U. Khan *et al.*, Chin. Phys. C **49**(7), 075105 (2025)
[20] A. Al-Badawi, Y. Sekhmani, and K. Boshkayev, Phys. Dark Univ. **48**, 101865 (2025)
[21] H. P. Saikia, M. M. Gohain, and K. Bhuyan, arXiv: 2504.13466
[22] D. Flores-Alfonso, B. A. González-Morales, R. Linares *et al.*, Phys. Lett. B **812**, 136011 (2021)
[23] K. Karshiboev, F. Atamurotov, A. Övgün *et al.*, New Astron. **109**, 102200 (2024)
[24] B. Eslam Panah, PTEP **2024**(2), 023E01 (2024)
[25] H. Kim, Phys. Rev. D **61**, 085014 (2000)
[26] M. Born and L. Infeld, Proc. Roy. Soc. Lond. A **144**(852), 425 (1934)
[27] G. W. Gibbons, AIP Conf. Proc. **589**(1), 324 (2001)
[28] I. Bandos, K. Lechner, D. Sorokin *et al.*, Phys. Rev. D **102**, 121703 (2020)
[29] V. Perlick, Living Rev. Relativ. **7**, 9 (2004)
[30] G. W. Gibbons and C. A. R. Herdeiro, Class. Quant. Grav. **18**, 1677 (2001)
[31] R. Ruffini, Y.-B. Wu, and S.-S. Xue, Phys. Rev. D **88**, 085004 (2013)
[32] B. P. Kosyakov, Phys. Lett. B **810**, 135840 (2020)
[33] T. Clifton, P. G. Ferreira, A. Padilla *et al.*, Phys. Rep. **513**, 001 (2012)
[34] C. G. Böhmer and E. Jensko, Phys. Rev. D **104**, 024010 (2021)
[35] S. Nojiri and S. D. Odintsov, Phys. Rep **505**, 59 (2011)
[36] T. P. Sotiriou and S.-Y. Zhou, Phys. Rev. Lett. **112**, 251102 (2014)
[37] S. Capozziello and M. de Laurentis, Phys. Rep. **509**, 167 (2011)
[38] E. Berti and *et al.*, Class. Quantum Grav. **32**, 243001 (2015)
[39] A. De Felice and S. Tsujikawa, Living Rev. Relativ. **13**, 3 (2010)
[40] K. Koyama, Reports on Progress in Physics **79**, 046902 (2016)
[41] L. Heisenberg, Phys. Rep. **796**, 001 (2019)
[42] J. Rayimbaev, R. C. Pantig, A. Övgün *et al.*, Annals of Physics **454**, 169335 (2023)
[43] B. Puliçe, R. C. Pantig, A. Övgün *et al.*, Class. Quantum Grav. **40**, 195003 (2023)
[44] S. Vagnozzi, R. Roy, Y.-D. Tsai *et al.*, Class. Quantum Grav. **40**, 165007 (2023)
[45] A. Uniyal, R. C. Pantig, and A. Övgün, Physics of the Dark Universe **40**, 101178 (2023)
[46] R. C. Pantig and A. Övgün, Annals of Physics **448**, 169197 (2023)
[47] F. Atamurotov, U. Papnoi, and K. Jusufi, Class. Quantum Grav. **39**, 025014 (2022)
[48] E. Ghorani, B. Puliçe, F. Atamurotov *et al.*, Eur. Phys. J. C **83**, 318 (2023)
[49] H. Hoshimov, O. Yunusov, F. Atamurotov *et al.*, Physics of the Dark Universe **43**, 101392 (2024)
[50] R. Kumar, S. U. Islam, and S. G. Ghosh, European Physical Journal C **80**, 1128 (2020)
[51] S. U. Islam, R. Kumara, and S. G. Ghosha, J. Cosmol. A. P **2020**, 030 (2020)
[52] D. Psaltis, Living Rev. Relativ. **11**, 9 (2008)
[53] E. Berti, V. Cardoso, and A. O. Starinets, Class. Quantum Grav. **26**, 163001 (2009)
[54] D. Psaltis and *et al.*, Phys. Rev. Lett. **125**, 141104 (2020)
[55] N. K. Johnson-McDaniel, arXiv: 1905.05565
[56] S. W. Hawking and G. F. R. Ellis, *The large-scale structure of space-time* (Cambridge: Cambridge University Press, 1973)
[57] K. S. Thorne, *Black holes and time warps: Einstein's outrageous legacy* (New York: W. W. Norton & Company, 1994).
[58] M. Volonteri, M. Habouzit, and M. Colpi, Nature Reviews Physics **3**, 732 (2021)
[59] R. Tsuda, R. Suzuki, and S. Tomizawa, arXiv: 2308.02146
[60] J. Barrientos, A. Cisterna, M. Hassaine *et al.*, Phys. Lett. B **860**, 139214 (2025)
[61] B. Eslam Panah, A. Rincon, and N. Heidari, arXiv: 2411.02907
[62] J. F. Plebański and S. Hacyan, Journal of Mathematical Physics **20**, 1004 (1979)
[63] V. Bozza, Phys. Rev. D **66**, 103001 (2002)
[64] K. S. Virbhadra and G. F. R. Ellis, Phys. Rev. D **62**, 084003 (2000)
[65] K. S. Virbhadra, Phys. Rev. D **79**, 083004 (2009)
[66] K. Akiyama and *et al.*, ApJL **875**, 44 (2019)
[67] V. Bozza and L. Mancini, General Relativity and Gravitation **36**, 435 (2004)